Revealing the magnetic proximity effect in EuS/Al bilayers through superconducting tunneling spectroscopy

E. Strambini,[1,*] V. N. Golovach,[2,3,4] G. De Simoni,[1] J. S. Moodera,[5] F. S. Bergeret,[2,3,†] and F. Giazotto[1,‡]

[1]*NEST Istituto Nanoscienze-CNR and Scuola Normale Superiore, I-56127 Pisa, Italy*

[2]*Centro de Fisica de Materiales (CFM-MPC), Centro Mixto CSIC-UPV/EHU, Manuel de Lardizabal 5, E-20018 San Sebastian, Spain*

[3]*Donostia International Physics Center (DIPC), Manuel de Lardizabal 4, E-20018 San Sebastian, Spain*

[4]*IKERBASQUE, Basque Foundation for Science, Maria Diaz de Haro 3, E-48013 Bilbao, Spain*

[5]*Department of Physics and Francis Bitter Magnet Laboratory, Massachusetts Institute of Technology, Cambridge, Massachusetts 02139, USA*

(Received 30 June 2017; published 4 October 2017)

A ferromagnetic insulator in contact with a superconductor is known to induce an exchange splitting of the singularity in the Bardeen-Cooper-Schrieffer (BCS) density of states (DoS). The magnitude of the splitting is proportional to the exchange field that penetrates into the superconductor to a depth comparable with the superconducting coherence length and which ranges in magnitude from a few to a few tens of tesla. We study this magnetic proximity effect in EuS/Al bilayers and show that the domain structure of the EuS affects the positions and the line shapes of the exchange-split BCS peaks. Remarkably, a clear exchange splitting is observed even in the unmagnetized state of the EuS layer, suggesting that the domain size of the EuS is comparable with the superconducting coherence length. Upon magnetizing the EuS layer, the splitting increases while the peaks change shape. Conductance measurements as a function of bias voltage at the lowest temperatures allowed us to relate the line shape of the split BCS DoS to the characteristic domain structure in the ultrathin EuS layer. These results pave the way to engineering triplet superconducting correlations at domain walls in EuS/Al bilayers. Furthermore, the hard gap and large splitting observed in our tunneling spectroscopy measurements make EuS/Al an excellent candidate for substituting strong magnetic fields in experiments studying Majorana bound states.

DOI: 10.1103/PhysRevMaterials.1.054402

I. INTRODUCTION

Europium sulfide is a classic Heisenberg ferromagnetic insulator (FI) with a Curie temperature of 16.7 K [1,2], which exceeds the transition temperature of most of the conventional superconductors. Together with EuO this material can be used as a very efficient spin-filter barrier [3,4]. Experiments carried out in the eighties have demonstrated that the exchange field of FIs, such as EuS and EuO, can split the excitation spectrum of an adjacent superconductor (S), such as an Al thin film [2,5,6]. This discovery opened up the way for performing spin-polarized tunneling measurements without the need of applying large magnetic fields [6]—a feature which is highly desirable when superconducting elements are present in an electronic circuit. More recently, EuS has also been used to create strong interfacial exchange fields in graphene [7] and topological insulators [8].

A renewed interest in studying ferromagnet/superconductor structures came with the development of superconducting spintronics [9]. The interaction between the superconducting condensate and the exchange field of a ferromagnet creates triplet superconducting pairs, which are able to carry nondissipative, spin-polarized currents [10]. The creation and control over the triplet correlations is intimately related with the magnetic configuration of the ferromagnet, with the domain walls playing an important role [11].

In the case of ferromagnetic insulators, a series of interesting phenomena have been predicted to occur in S/FI structures with spin-split density of states (DoS), such as huge thermoelectric effects [12–16] and highly efficient spin and heat valves [17–20]. These effects can be exploited for creation of spin-polarized currents with a high degree of polarization [17,21,22], for on-chip cooling at the nanoscale [23,24], and for low-temperature thermometry and highly sensitive detectors and bolometers [25].

A spin-split superconducting DoS is also an essential ingredient in Majorana-based quantum computing [26,27]. The exchange splitting of the Bardeen-Cooper-Schrieffer (BCS) singularity observed in EuS/Al bilayers is as large as the splitting caused by an external magnetic field of several tesla. Therefore, replacing the superconductor by an EuS/Al bilayer or another FI-S carefully-designed structure should allow one to reduce significantly or, in certain cases, even avoid the use of magnetic fields in experiments searching for Majorana fermions. This possibility becomes especially attractive at the production cycle, since having to apply strong magnetic fields is impractical, whereas the magnetization of an island of FI can be manipulated on-chip through electric currents via local magnetic fields or a spin-transfer torque.

All these applications need a sizable splitting of the superconducting DoS in a large temperature range below the superconducting critical temperature (T_c). A first and essential step towards controlling the magnitude of the exchange splitting is to understand the magnetic proximity effect induced by the FI material in an adjacent superconductor. Although different FI/S systems have been studied for almost three decades, there is still a great deal of controversy about the relation between the magnetic configuration of the EuS and the spin splitting induced in the superconductor [2,28]. Moreover, very few articles focus on the behavior of the EuS/Al bilayers at temperatures well below 1 K.

Here, we present an accurate tunneling spectroscopy of the superconducting DoS of an EuS/Al bilayer in the temperature

*elia.strambini@sns.it

†sebastian_bergeret@ehu.eus

‡francesco.giazotto@sns.it

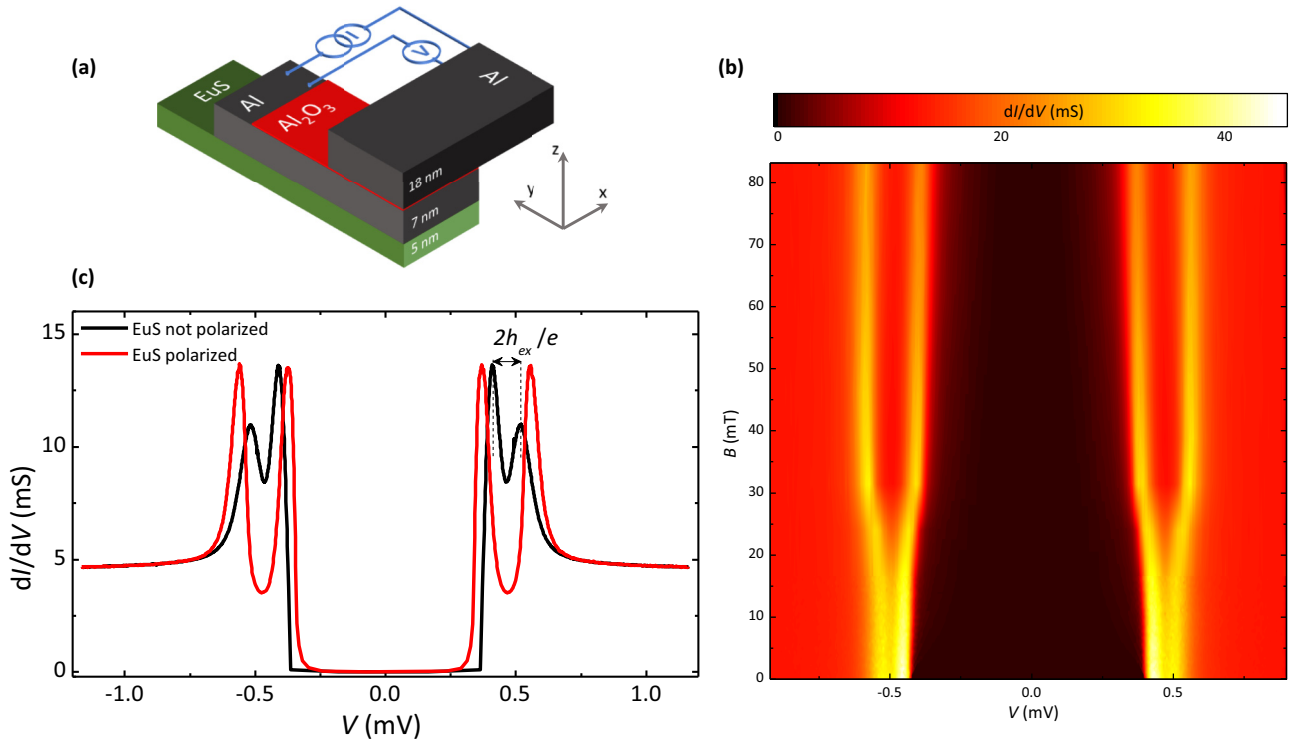

FIG. 1. Junction layout and tunneling spectroscopy of the first magnetization. (a) Sketch of the cross bar forming the EuS(5)/Al(7)/Al_2O_3/Al(18) vertical tunnel junction (the thickness is in nanometers). The area of the junction is a square of 290 × 290 μm^2. (b) Evolution of the differential conductance, obtained from the numerical derivative of the I-V curves, as a function of the voltage drop (V) and in-plane magnetic field (B) during the first magnetization of the EuS layer. (c) Comparison between the differential conductance of the tunnel junction measured at zero field before (black curve) and after (red curve) the magnetization of the EuS layer. All the measurements were taken at 25 mK.

range 30 mK–1.2 K. The exchange splitting observed in the Al layer reaches up to 0.2 meV in the presence of a moderate in-plane magnetic field of 30 mT, which is applied in order to align the magnetic domains of the EuS. Once magnetized, the spin splitting is also clearly observed at zero applied field. Most notable, however, is the fact that the experimental data exhibits the splitting even in the demagnetized phase of the EuS, i.e., even before the first application of a magnetic field. Moreover, the line shape of the BCS singularity is considerably reconstructed as compared to the standard BCS line shapes observed in the magnetically ordered state: in a homogeneous exchange-split superconductor, the total DoS is a sum of a spin-up and a spin-down BCS DoS, shifted in energy with respect to each other by the exchange splitting, resulting in a four-peak structure with the outer peaks higher than the inner ones [6]. However, our measurements in the demagnetized phase of the EuS show that the peak heights have the opposite asymmetry as compared to the homogeneous case.

In order to understand the experimental observations, we model the EuS as a periodic structure of magnetic domains of different sizes and compute the DoS of the Al film with the help of the quasiclassical Green's function formalism. Our analysis shows that an exchange splitting in the DoS of the Al layer before the magnetization of the EuS can only be obtained if the EuS layer consists predominantly of large domains, i.e., much larger than the superconducting coherence length. Yet, the fact that the BCS singularity is considerably reshaped in the demagnetized case indicates that domain walls are not that rare, and contribute sizeably to the tunneling spectroscopy. We identify the main physical processes responsible for the reconstruction of the BCS singularity around a domain wall and make predictions about a possible scanning tunneling microscopy of the EuS/Al bilayer.

Further information about the magnetic configuration of EuS can be extracted from the temperature dependence of the exchange splitting. Surprisingly, there is a 10% reduction of the splitting when the temperature is varied from 30 to 900 mK. We attribute this large change of the splitting over a temperature range much smaller than the Curie temperature to the Al/EuS interface that may consist of single localized spins (Eu atoms) coupled to the EuS layer only by one bond. We support this hypothesis by a calculation of the average magnetic moment at the interface.

Finally, we use the well-pronounced gap to achieve a large tunneling magnetoresistance (TMR) at the magnetization reversal point $H_c \approx 18.5$ mT, obtaining 200 % at $T = 30$ mK and 700 % at $T = 850$ mK. Notably, these large TMR values are achieved using only one magnetic layer. Apart from serving as a measurement of the figure of merit for the hardness of the gap in a functional FI/S device, the large observed TMR values suggest that Al/EuS systems can be used as building blocks for superconducting spin-based electronic devices.

II. SAMPLES AND MEASUREMENTS

The tunneling spectroscopy of the EuS/Al bilayer has been done on EuS(5)/Al(7)/Al_2O_3/Al(18) tunnel junctions

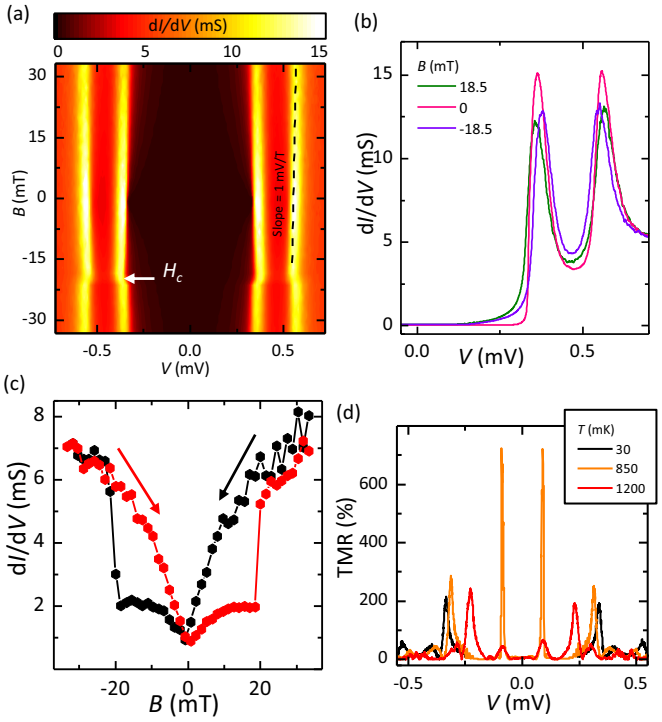

FIG. 2. Hysteretic cycle of the tunnel junction. (a) Full evolution of the $dI/dV(V)$ of the tunnel junction traced from 30 to -30 mT. The dashed line is a guide to the eye following the peak maximum. (b) $dI/dV(V)$ for selected values of B. (c) Forward trace ($B: 30 \rightarrow -30$ mT, black dots) and backward trace ($B: -30 \rightarrow 30$ mT, red dots) of the tunneling conductance extrapolated at $V = 335\mu$V. The measurements of (a)–(c) were taken at 30 mK. (d) Tunneling magnetoresistance (TMR) values evaluated at 30, 850, and 1200 mK.

(thickness in nanometers). Samples consist of cross bars fabricated by electron-beam evaporation on in situ metallic shadow mask (see Appendix for fabrication details). The typical area of the FI/S/I/S junction is $290 \times 290\ \mu\text{m}^2$. The tunneling spectroscopy of the junctions is obtained by measuring the V-I characteristics in a dc four-wire setup sketched in Fig. 1(a) from which the differential conductance is evaluated via numerical differentiation. The cross-bar junctions are characterized at cryogenic temperatures, down to 25 mK, in a filtered cryogen-free dilution refrigerator.

III. RESULTS

Samples are first cooled down from room temperature to 30 mK in a nonmagnetic environment. Surprisingly, before the application of any magnetic field, the dI/dV versus V shows four clear peaks indicating an exchange splitting in the DoS of the bottom Al layer (as shown in Figs. 1(b) and 1(c) for two similar devices). The symmetry and position of these peaks, in a first approximation, can be well described within the Tedrow and Meservey theory [6] of quasiparticle spin-polarized tunneling, for which four superconducting peaks are expected at the voltages

$$eV_{\text{peak}} \simeq \pm(\Delta_1 + \Delta_2) \pm h_{\text{ex}}, \qquad (1)$$

where Δ_i is the pairing potential of each superconductor forming the junction, e is the electron charge, and h_{ex} is the exchange energy induced in the bottom Al layer in contact with the EuS film. Assuming equal pairing potentials in the two Al layers, the measurement is compatible with $\Delta \approx 230\ \mu$eV and an exchange splitting $2h_{\text{ex}} \approx 110\ \mu$eV. The latter is equivalent to an effective magnetic field $B_{\text{ex}} = 2h_{\text{ex}}/g\mu_B \sim 1$ T, where $g \approx 2$ is the Landé g-factor, and μ_B is the Bohr magneton. Energy splittings comparable in magnitude have been reported in measurements on similar junctions, but only after applying a magnetic field [29].

Next we apply an in-plane magnetic field (B) to the sample. As shown in Fig. 1(b), the separation between the peaks in the dI/dV increases showing a saturation above 30 mT. The effective spin splitting increases up to $\sim$190 μeV (which would correspond to a magnetic field of $\sim$1.6 T) and is preserved even without the presence of an external magnetic field [see the red plot of Fig. 1(c)]. The superconducting pairing potential Δ is almost unaffected. The enhancement of the spin splitting can be associated with the increased magnetization of the EuS layer.

Not only the position, but also the shape of the conductance peaks is different before and after the first magnetization of the EuS film. In the demagnetized phase, the amplitude of inner peaks (at $|V| < 0.5$ mV) is larger with respect to the outer ones. To the best of our knowledge, this behavior has never been reported so far and cannot be described by the over-simplified Tedrow-Meservey model, which assumes an homogeneous exchange field induced in the superconductor [6]. Below we demonstrate that this behavior can only be explained by taking into account the multidomain structure of the polycrystalline EuS layer, which leads to an inhomogeneous exchange field.

Another striking observation is the sharpness of the tunneling conductance at the gap edge [black curve in Fig. 1(c)] in the demagnetized phase, in contrast to a smoother transition after the first magnetization (red curve). These two different behaviors can be explained by means of the stray field generated by the domain structure of the EuS. In the demagnetized phase the EuS consists of domains with independent magnetization pointing in random directions [see sketch in Fig. 4(a)]. Seen from the Al-layer, the contributions to the field from different domains, being randomly oriented, compensate each other and results in a small stray field. In contrast, in the magnetized phase, although the number of domains can be smaller, more domains are aligned and hence their contribution sum up enhancing the stray field. This field acts as a pair breaking mechanism for the superconductor and broadens the BCS peaks. An external magnetic field has the same effect as can be seen in Figs. 2(a) and 2(b). One clearly sees a larger broadening when a finite field is applied.

After the first magnetization of the EuS film, the magnetic-field dependence of the tunneling conductance follows the typical ferromagnetic hysteretic behavior. Figure 2(a) shows the typical evolution of the $dI/dV(V)$ extracted from the junction I-V at finite in-plane magnetic fields. The curves show a clear spin splitting, which increases when the field is applied. This splitting is as large as $\sim$1 mV/T [see dashed line in Fig. 2(a)] and cannot be attributed only to the Zeeman splitting caused by the external field [28]. The reason for the

large splitting observed is that the field tends to enlarge the size of the magnetic domains and hence the averaged exchange field seen by the electrons over the Cooper pair size, as explained by our model below.

By reversing the field direction ($B < 0$), i.e., antiparallel to the EuS magnetization, the number and size of the domains with parallel magnetization is reduced. This leads to a decrease of the spin splitting down to the coercive $H_c \sim -18.5$ mT [see Fig. 2(b)]. The discontinuity in the conductance peaks observed at this value of the field is a manifestation of the magnetization switching of the EuS. Further increase of the applied field in the negative direction restores the maximum exchange splitting. By retracing back B a similar hysteretic behavior is observed with a coercive field of opposite sign ($H_c \sim 18.5$ mT).

The hysteretic behavior together with the strong suppression of the differential conductance at subgap voltages ($|eV| < 2\Delta - h_{ex}$) suggest the possibility to operate this structure as a magnetic switching device. Notably, such a device is based on a single ferromagnetic layer and could, in principle, be exploited as a *permanent* memory element. The performance of the junction as a nonvolatile memory can be quantified by its tunneling magnetoresistance (TMR) evaluated from the hysteretic spectra of the $dI/dV(B)$ curves shown in Fig. 2(c) and defined as

$$\mathrm{TMR} = \mathrm{Max}(G_{fw}/G_{bk}, G_{bk}/G_{fw}) - 1,$$

where G_{fw} (G_{bk}) is the forward (backward) differential conductance. As shown in Fig. 2(d), the TMR at 30 mK can exceed 200% by tuning the bias voltage in the subgap energy regime, $V \simeq 335\ \mu$V, corresponding to an active voltage range for which the junction switches between the insulating state (subgap conductance) and the conducting state, depending on the magnetic configuration of the EuS. Furthermore, the figure shows that such a high TMR value is preserved when increasing the temperature up to $T \lesssim T_c$ as, in this temperature window, thermal broadening is negligible compared to the energy scale of the exchange splitting. In addition, above 0.5 K the TMR shows an interesting feature in the subgap region (around $V \simeq 80\ \mu$V) that is even more sensitive to the magnetic switching (TMR $> 700\%$). This subgap feature stems from the presence of the superconducting matching peaks, which are activated by the temperature and exchange field in these junctions. These can be appreciated in Fig. 3(a) showing the differential conductance $dI/dV(V)$ measured at different temperatures. As predicted by the quasiparticle spin-polarized tunneling theory, the thermal activation enhances the subgap matching peak at $|eV| \simeq \Delta_1 - \Delta_2 + h_{ex} \simeq 80\ \mu$V. The position of these additional maxima provides an alternative estimation of the energy splitting, which is consistent with the BCS peaks splitting observed at higher voltages.

From the tunneling conductances measured at different temperatures we extracted the temperature evolution of both the exchange energy and the coercive field in a region of temperatures never explored so far for EuS. These results are presented in Fig. 3(b). Both the exchange energy and the coercive field increase by lowering the temperature, suggesting that the ferromagnetic ordering of the EuS and, in turn the resulting magnetic proximity effect, are affected even in a temperature range much lower than the Curie temperature of the EuS. As discussed below, this anomalous behavior can be attributed to the magnetic properties of weakly coupled Eu atoms at the interface with the Al layer.

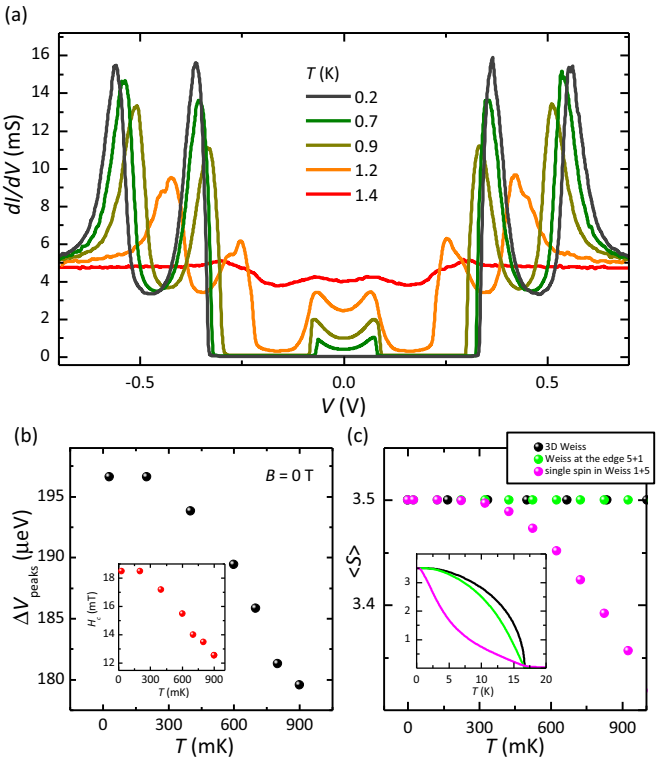

FIG. 3. Temperature evolution of the tunnel junction behavior. (a) Differential conductance $dI/dV(V)$ of the tunnel junction measured at different bath temperatures in zero magnetic field and after the magnetization of the EuS layer. (b) Temperature evolution of the exchange splitting extracted form the $dI/dV(V)$ characteristics measured at zero field. (Inset) Temperature evolution of the coercive field (H_c) extracted form the switching of the tunneling conductance [as shown in Fig. 2(a)]. (c) Theoretical temperature dependence of the EuS averaged spin $\langle S \rangle$ calculated using different approaches. (Inset) Evolution of $\langle S \rangle$ in the full temperature range.

IV. THEORETICAL DESCRIPTION OF THE MAGNETIC PROXIMITY EFFECT

In all previous works on EuS/Al, the spin splitting is modeled by assuming an homogeneous exchange energy h_{ex}. In such a situation, the DoS of the Al-layer can be approximated by the sum of the DoS for spin up and spin down:

$$N_s^{\mathrm{hom.}} = \frac{1}{2} \sum_{\sigma=\pm 1} N_{\mathrm{BCS}}(E + \sigma h_{ex}) \,, \qquad (2)$$

where $N_{\mathrm{BCS}}(E) = |\,\mathrm{Re}[(E + i\Gamma)/\sqrt{(E + i\Gamma)^2 - \Delta^2}]|$ is the usual BCS DoS normalised with respect to the total DoS in the normal state and $\Gamma > 0$ is the Dynes parameter describing inelastic scattering. The exchange energy $\pm h_{ex}$ describes the splitting observed in the tunneling conductance of the FI/S-I-S tunnel junctions and the shape of the $dI/dV(V)$ derived from Eq. (2) is very similar to the one observed in the magnetized case [see, e.g., red curve in Fig. 1(c)].

In the demagnetized case, although the total magnetization is negligibly small, a clear splitting is observed in the experiment [black curve in Fig. 1(c)]. However, the shape of the $dI/dV(V)$ curve is very different from the one observed after the first magnetization of the EuS, and hence cannot be described by the homogeneous DoS given by Eq. (2). In other words, if one would assume that the enhancement of the splitting after magnetizing the EuS layer is due to the increase of a homogeneous exchange h_{ex} in Eq. (2), one would not be able to explain the reversed relative height of the inner and outer peaks in Fig. 1(c).

The main assumption for our theoretical model is that the EuS consists of magnetic domains, typical for ferromagnetic materials. Indeed, it is known that EuS films are polycrystalline and consist of an ensemble of crystallites with intrinsic magnetization [30]. In the absence of an applied field and before the first magnetization, each crystallite can be regarded as a single-domain magnet with their ensemble having random magnetization orientation relative to each other [see Fig. 4(a)]. The typical size of such domains can be on the order of several hundreds of nanometers, and depends on the growth conditions. Because of a weak anisotropy, when a magnetic field is applied, the magnetic moments of the crystallites tend to orient themselves parallel to the applied field, forming large domains leading to homogeneous magnetization.

The spin splitting observed in the differential conductance of FI/S-I-S junctions is attributed to the magnetic proximity effect, i.e., to the exchange interaction between the spin moment of the Eu ions $\mathbf{S}$ and the spin density of conducting electrons $\mathbf{s}(\mathbf{r})$. To describe this interaction we assume a simple exchange Hamiltonian:

$$H_{ex} = -J \sum_j \boldsymbol{S}_j \cdot \boldsymbol{s}(\boldsymbol{r}_j), \tag{3}$$

where J is the interfacial coupling constant. By averaging Eq. (3) in the ferromagnetic state of the EuS, we obtain the local exchange coupling

$$\hat{h}_{\rm ex}(x,y,z) = -\tfrac{1}{2} J n_{\rm 2D} \hat{\boldsymbol{\sigma}} \cdot \boldsymbol{S}(x,y)\delta(z - z_M)\,. \tag{4}$$

Here, $n_{\rm 2D}$ is the two-dimensional concentration of Eu ions accessible to the Al electrons at the interface, $\boldsymbol{S}(x,y)$ is the average value of the interfacial local moment, $\hat{\boldsymbol{\sigma}}$ are the Pauli

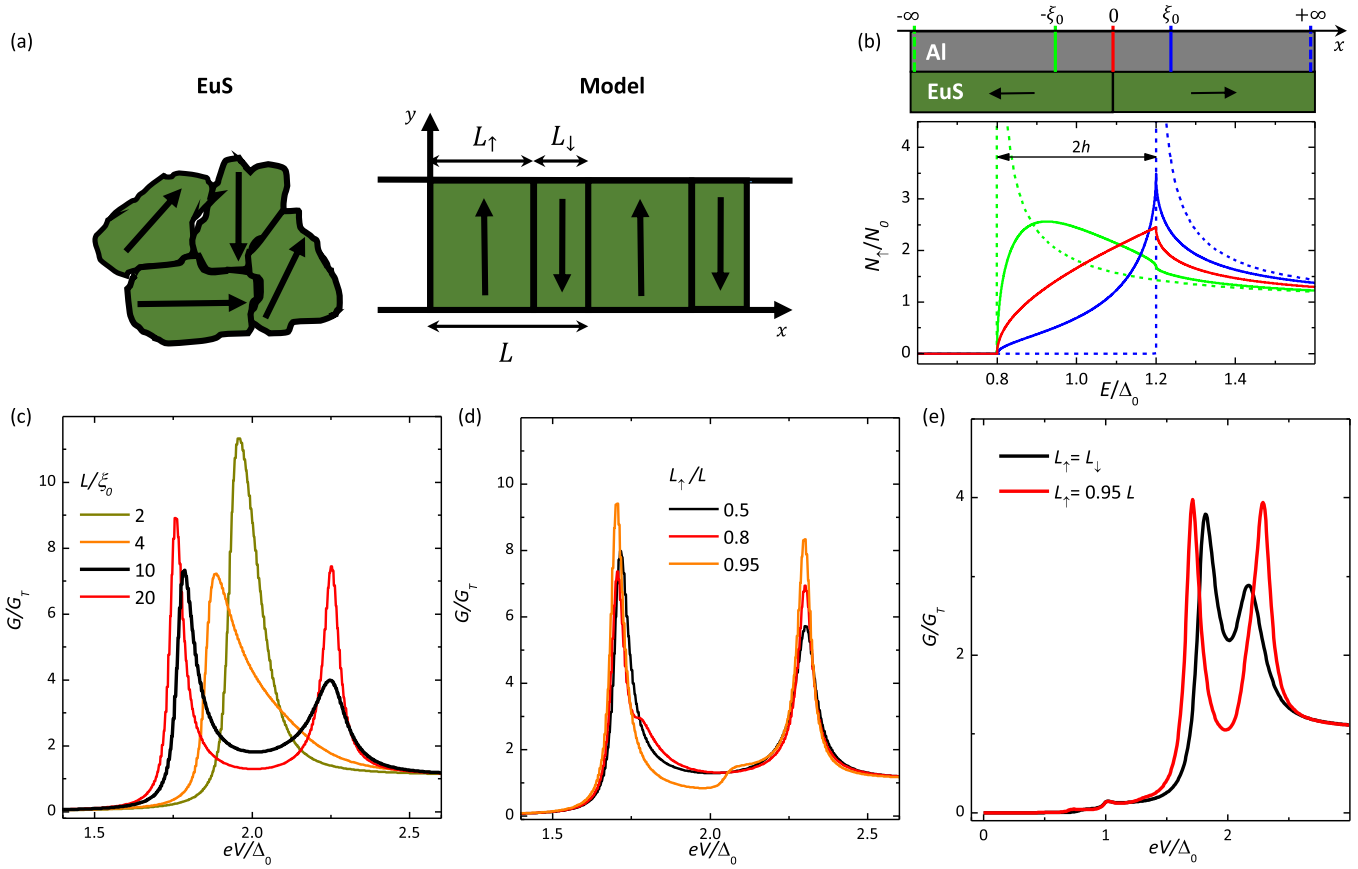

FIG. 4. Theoretical model of the tunneling conductance. (a) Sketches showing (left) the polycrystalline structure of the EuS and (right) the effective model of alternating up-down domains used in the simulation. We consider two lengths $L_\uparrow$ and $L_\downarrow$ and define $L = L_\uparrow + L_\downarrow$. The demagnetized phase is described by $L_\uparrow = L_\downarrow$, whereas after magnetization $L_\uparrow \gg L_\downarrow$. (b) Local density of states of the Aluminum on top of a two semi-infinite domain structure. The dashed lines show the spin-split BCS DoS deep inside the domains at $x \to -\infty$ (blue) and $x \to +\infty$ (green). By approaching the domain wall the DoS changes. Line traces of the plot the solid lines are taken at $x = -\xi_0$ (blue), $x = 0$ (red), and $x = \xi_0$ (green). (c) Averaged tunneling conductance calculated for an infinite stripe of balanced up/down domains $L_\uparrow = L_\downarrow$ then describing the demagnetized EuS calculated for different domain size (L), $\Gamma = 0.01\Delta$ and $T = 0.01T_c$. (d) Evolution of the tunneling conductance calculated at different magnetizations $L_\uparrow$ and $L = 10\xi_0$, $\Gamma = 0.01\Delta$, and $T = 0.01T_c$. (e) Tunneling conductance calculated for a demagnetized phase, made of six different domains, (black plot) and for a fully magnetized phase (red plot) including magnetic scattering.

spin matrices, and z_M is the position of the EuS/Al interface. By assuming such effective exchange interaction, the spectrum of the superconductor adjacent to the EuS can be determined from the quasiclassical Green's function, $\check{g}$, that in the diffusive limit satisfies the Usadel equation [10,31]:

$$\hbar D\nabla\check{g}\nabla\check{g} + iE[\tau_3,\check{g}] - i[\tau_3\hat{h},\check{g}] + \Delta[\tau_2,\check{g}] = [\check{\Sigma},\check{g}], \quad (5)$$

under the constraint $\check{g}^2 = \check{\mathbb{1}}$ and with suitable boundary conditions (details of the notations and the boundary problem are given in Appendix). The exchange energy $\hat{h}$ entering this equation consists of the Zeeman term and an interfacial exchange term, $\hat{h}(\boldsymbol{r}) = \frac{1}{2}g\mu_B\hat{\boldsymbol{\sigma}}\cdot\boldsymbol{B} + \hat{h}_{\rm ex}(\boldsymbol{r})$. The term in the right-hand side (r.h.s) of (5), describes possible sources for inelastic scattering or pair-braking mechanisms described by the self-energy $\check{\Sigma}$. In the most simple case, one describes inelastic scattering by the energy independent Dynes parameter such that $\check{\Sigma} = \Gamma\tau_3$.

Equation (5) determines the length scales over which the spectral properties of the Aluminum are modified. This scale is of the order $\sim\xi_0 = \sqrt{\hbar D/\Delta}$. If we assume that the thickness of the Al layers is small compared to this length, we can integrate Eq. (5) over the thickness (z direction) and reduce the 3D to a 2D problem (details in Appendix). Specifically, given a magnetic configuration, S(x,y) of the EuS at the interface $z = z_M$ one has to solve Eq. (5) to determine the local DoS of the Al film from the equation:

$$N_\sigma(E,x,y) = \frac{N_0}{2}\,\mathrm{Re}\,\{\mathrm{Tr}\,[g_\sigma(E+i0,x,y)\tau_3]\}, \quad (6)$$

where Tr[...] stands for the trace in the Nambu space and N_0 is the total DoS in the normal state. It is easy to check that in the homogeneous case the solution of the Usadel equation gives the simple spin-split BCS DoS of Eq. (2). In order to describe the polycrystalline phase of the EuS with random magnetization we model it by assuming a stripe of domains with alternating up and down magnetization [see Fig. 4(a)]. The relative size between up and down domains will depend on the magnetization state of the EuS. This reduces further the problem to 1D. As we shall see, even with this simplification we are able to catch most of the experimentally observed conductance features.

It is instructive to focus first on the problem of two semi-infinite domains with opposite magnetization and a single domain wall at $x = 0$. This case in fact can be solved analytically. In Fig. 4(b), we show the local DoS (for one spin species) calculated from the Usadel equation at different points. As expected, deep in the bulk of the domains, ($|x| \gg \xi_0$) the density of states is a BCS peak shifted on each side of the domain wall, $N_\uparrow(E,\pm\infty) = N_{\rm BCS}(E \pm h_{\rm ex})$ (dashed lines). The BCS singularity is recovered only asymptotically with $x \to \pm\infty$. On a length scale ξ_0 around the domain wall, there is a crossover from the two shifted BCS curves to a "shark-fin" shape at the domain wall, $x = 0$. It is important to emphasize that the inner "peak" at $E = \Delta - h$ looks as being shifted to larger energies when moving towards the domain wall, whereas the features at $E = \Delta + h$ remain at the same energy. These features, which will be used below to understand the dI/dV curves, could be verified by measuring the local DoS with, for example, a scanning tunneling microscope [32,33]. Here we perform a planar tunneling spectroscopy, with a large contact area between the FI/S bilayer and the superconducting electrode [see Fig. 1(a)]. This means, in particular, that by measuring the tunneling differential conductance of the junctions we obtain information about the DoS averaged over the area of the tunnel barrier and the two spin species ($\bar{N}(E) = \sum_\sigma < N_\sigma(E,\sigma,x) >_x$):

$$\frac{dI}{dV}(V) = \frac{G_T}{e}\frac{d}{dV}\int dE\, N_{\rm BCS}(E+eV)\bar{N}(E) \times [f(E) - f(E+eV)]\,, \quad (7)$$

where G_T is the normal-state conductance of the tunneling barrier and $f(E)$ is the Fermi function. To extend the model to a realistic multidomain structure we solved numerically the Usadel equation and calculated the average DoS for an infinite stripe [see Fig. 4(a)] made of two domains of length $L_\uparrow$ and $L_\downarrow$ repeated with $L = L_\uparrow + L_\downarrow$ periodicity. The ratio $L_\uparrow/L_\downarrow$ determines the total magnetization of the EuS. In the demagnetized phase we have $L_\uparrow/L_\downarrow = 1$, whereas after the magnetization we assume $L_\uparrow/L_\downarrow \gg 1$. The other important parameter of the theory is the ratio L/ξ_0 that, as we see below, determines crucially the shape of the dI/dV(V) curves obtained by the tunneling spectroscopy.

For the demagnetized phase of EuS we assume that $L_\uparrow = L_\downarrow$ and explore the role of the domain size on the tunneling conductance. This is shown in Fig. 4(c), where $dI/dV(V)$ curves are shown for different values of L/ξ_0. Despite the fact that the total magnetization of the EuS is zero, a clear splitting is visible for large domains $L > 4\xi_0$ and reaches the asymptotic value $2h_{ex}$ above $20\xi_0$. These results suggest a typical domain size of $\sim 10\xi_0$ in the EuS films. Moreover, our model also described correctly the relative heights of the peaks in the demagnetized phase.

After applying the magnetic field the ratio $L_\uparrow/L_\downarrow$ is increased. By fixing the period of the structure $L = L_\uparrow + L_\downarrow = 10\xi_0$, we show in Fig. 4, the $dI/dV(V)$ for different values of $L_\uparrow/L_\downarrow$. Our results clearly show that the separation between the spin-split peaks increases by increasing the ratio $L_\uparrow/L_\downarrow$ which modifies also the relative heights of the peaks that tends to the case of homogeneous field result at $L_\uparrow/L_\downarrow \to \infty$. Despite the fact that the model assumes a unique domain size for each spin species, most features of Fig. 1 are caught within this model.

There are, however, two main discrepancies between the theoretical results and the measurements: on the one hand, the peaks observed experimentally show a much larger broadening than seen in the calculated ones. This discrepancy is easy to understand recalling that in a real situation magnetic disorder, spin-orbit coupling, and the effect of stray fields will broaden all the features [34]. These effects are energy dependent (see the r.h.s of Eq. (5)] and for simplicity have not been included in the simulation. Instead, we modeled the inelastic scattering by the energy independent Dynes parameter $\Gamma = 0.01\Delta$. On the other hand, there is a more important discrepancy if one compares the results of our model, Fig. 4(d), with the measurements before and after the first magnetization, Fig. 1(c). In the latter, we clearly see that by magnetizing the EuS layer the splitting peaks move symmetrically with respect to the voltage $eV = 2\Delta$. In contrast, our simulations, Fig. 1(c), shows that only the inner peak is shifted by changing the value

$L_\uparrow/L_\downarrow$. The voltage at which the outer peak appears does not change though, in accordance with the result for the DoS using the two infinite domains model, Fig. 4(b).

The latter discrepancy is a consequence of the assumption we made that the sizes of all up and down domains is unique. In reality, the size of the domains follows certain distribution with an average domain size given, according to our previous results to $\sim 10\xi_0$. In order to describe this situation within our model, we assume for example that inside the up(down) domain there is a smaller down(up) domain. Figure 4(e) shows the resulting tunneling conductance obtained by assuming small domains with a size 10% of the host domains. The effect of the small domains embedded in the larger ones is to reduce the magnitude of the effective spin splitting that leads to the symmetric shift of the peaks. In order to broaden the peaks we have used a larger Dynes parameter, $\Gamma = 0.03\Delta$. Being independent of the energy its inclusion leads to subgap features, which can be neglected.

V. TEMPERATURE DEPENDENCE OF THE EXCHANGE COUPLING

The last striking feature to be explained is the strong temperature dependence of the exchange coupling observed in Fig. 3(b). The surprising issue is the small temperature window over which the exchange field changes even at such low temperatures. This energy scale is clearly not related to the Curie temperature of the EuS layer, which is more than one order of magnitude larger. A similar feature was also reported in Ref. [28] when the sample was immersed in a magnetic field of 50 mT. The feature was attributed to a "thermally activated" spin-relaxation mechanism, although the authors did not elaborate this hypothesis. We provide here an alternative and more plausible explanation.

According to our description of the magnetic proximity effect, the exchange field is proportional to the average (localized) spin, Eq. (4). In order to estimate this average we have calculated the magnetization for a cubic lattice with $S = 7/2$ in the nodes and with Heisenberg exchange interaction between nearest neighbors. For the exchange coupling of $J = 0.0688$ meV, we can recover the EuS Curie temperature (16.7 K), using the self-consistency equations of the RPA theory. This calculation [see Fig. 3(c)] demonstrates that the change of magnetization in going from 30 to 900 mK is negligibly small ($<0.4\%$) in the bulk of the EuS film. But at the surface, the effect might be somewhat larger, because the spins have five nearest neighbors and not six as in the bulk. To verify how large this change is, we compute within the Weiss mean-field theory the surface average spin. The change becomes 10^{-6} in the usual Weiss theory, and 10^{-5} in the relaxed at the surface Weiss theory. Thus, in both cases, the average spin do not have any special characteristic scale other than the usual Curie temperature, and therefore one cannot explain the change of h_{ex} observed in Fig. 3(b).

An alternative explanation is that the observed 10% reduction of the effective splitting in going from 25 to 900 mK could be attributed to the increase of ξ_0, and hence to the reduction of the average exchange field. This could be correct provided the $B = 0$ data in Fig. 3(b) was taken "before" magnetization. But this is not the case. Moreover, in Ref. [28] the same behavior was observed in the presence of a large magnetic field.

In order to understand this issue we propose the following scenario: most likely, the EuS surface has a portion of spins which do not have the 5+1 coordination (here 1 stands for the Al atom). There should be spins which stand out of the lattice and are coupled to the rest of the EuS by just one single bond with the same exchange $J = 0.0688$ meV as the bulk Eu spin. These loose surface spins correspond to a 1+5 coordination (now 5 stands for Al atoms and 1 for Eu). For such spins, we get the magenta curve in the plot of Fig. 3(c). The new characteristic temperature scale of the down bending of the curve is basically given by J, which could in principle be even smaller than that for the lattice. This explains the change of the average spin, and thereby of the effective exchange field over such a small temperature window.

VI. CONCLUSIONS

In summary, by combining tunneling conductance measurements and a microscopic model based on the quasiclassical Green's functions we gave an exhaustive description of the magnetic proximity effect in ferromagnetic insulator/superconductor EuS/Al bilayers. By comparing our calculations of the density of states and tunneling conductance with the measurements we conclude that the EuS film consists of magnetic domains with sizes larger than the superconducting coherence length. In the demagnetized phase of the EuS layer, each of these domains has an independent magnetic moment randomly oriented and causes an exchange field parallel to the local magnetization. Because of the large mean size of the domains in comparison to the coherence length of the superconductor, even before applying any magnetic field, the spectrum of the Al layer shows a well-defined spin splitting. By applying a magnetic field, the mean size of the domains with magnetization parallel to the applied magnetic field increases. This manifests as an enhancement of the spin splitting of the density of states of the superconductor and a modification of $dI/dV(V)$ curves towards the ones assumed in previous works for an ideal homogeneous magnetization. Moreover, the observed spin splitting, evolving in a temperature range much smaller than the Curie temperature of the bulk EuS, reveals the presence of weakly bound spins at the interface of the EuS/Al. Because of the large spin splitting observed even in the absence of any applied magnetic field, the EuS/Al material combination is an excellent platform for the development of devices requiring the coexistence of superconducting correlations and spin-splitting exchange fields, as, for example, in the field of Majorana-based quantum computation.

ACKNOWLEDGMENTS

Partial financial support from the European Union's Seventh Framework Programme (FP7/2007-2013)/ERC Grant 615187-COMANCHE is acknowledged. The work of E.S. is funded by the Marie Curie Individual Felloship MSCA-IFEF-ST No. 660532-SuperMag. The work of G.D.S. is funded by Tuscany Region under the FARFAS 2014 project SCIADRO. The work of F. S. B. and V. G. was supported by Spanish Ministerio de Economía y Competitividad (MINECO)

through Project No. FIS2014-55987-P. J.S.M. acknowledges the support from NSF Grants No. DMR-1207469 and No. DMR-1700137, ONR Grants No. N00014-13-1-0301 and No. N00014-16-1-2657 and John Templeton Foundation grant.

APPENDIX: METHODS

1. Sample fabrication

The structure of the investigated magnetic tunnel junctions is EuS(5)/Al(7)/Al_2O_3/Al(18) (the thickness are in nanometers), where the materials are listed in the order in which they were deposited. The junctions were fabricated in a vacuum chamber with a base pressure 2×10^{-8} Torr using *in situ* shadow evaporation on metal masks. To facilitate the growth of smooth films, a thin Al_2O_3 (1 nm) seed layer was deposited onto glass substrates, which were chemically cleaned exsitu and oxygen-plasma cleaned insitu before the growth of the films. The electrodes Al films were evaporated from resistive W coil, whereas for EuS film bulk pellet was used for electron-beam evaporation. The Al_2O_3 barrier was formed by plasma oxidization of the first Al(7) film surface. Film thicknesses were measured during the film growth using quartz crystal sensor. The substrate-holding Cu block was cooled by flowing liquid nitrogen for depositing the films on a cooled surface (∼80 K). Subsequently, the structure was warmed to room temperature in ultrahigh vacuum before taking out the thin-film junction (with protective Al_2O_3 capping layer) for transport measurements.

2. Brief description of the theory

We describe the electronic properties of the superconducting film with the help of the quasiclassical Green function $\check{g}(\boldsymbol{r})$, obtained as a solution of the Usadel equation, Eq. (5) [10,31]. We described inelastic scattering by the energy independent Dynes term on the r.h.s:

$$\frac{D}{2}\sum_{\alpha}\partial_\alpha[\check{g},\partial_\alpha\check{g}] + iE[\tau_3,\check{g}] - i[\tau_3\hat{h},\check{g}] + \Delta[\tau_2,\check{g}] = [\Gamma\tau_3,\check{g}]. \tag{A1}$$

Here, D is the diffusion constant, E is the quasiparticle excitation energy, Δ is the superconducting gap, and the sum runs over the spacial directions ($\alpha = x,y,z$). We use two sets of Pauli matrices, $\boldsymbol{\tau}$ and $\hat{\boldsymbol{\sigma}}$, to represent quantities in the Nambu and spin spaces, respectively. A check accent ($\check{g}$) denotes a 4×4 matrix in the direct product of the spin and Nambu spaces, whereas a hat accent ($\hat{h}$) denotes a 2×2 matrix in the spin space only. The exchange field $\hat{h}(\boldsymbol{r})$ consists of the Zeeman term and an interfacial exchange term:

$$\hat{h}(\boldsymbol{r}) = \tfrac{1}{2}g\mu_B\hat{\boldsymbol{\sigma}}\cdot\boldsymbol{B} + \hat{h}_{\rm ex}(\boldsymbol{r}), \tag{A2}$$

where $g \approx 2$ is the Al g-factor, μ_B is the Bohr magneton, $\boldsymbol{B}$ is the magnetic field, and $\hat{h}_{\rm ex}(\boldsymbol{r})$ is the exchange field coming from the magnetic interface, which is inhomogeneous in space.

The boundary conditions for $\check{g}$ inside the Al film at its upper ($z = 0$) and lower ($z = -d$) surfaces are obtained by infinitesimal integration across each interface, assuming that $\check{g}$ vanishes identically both in the Al_2O_3 barrier ($z > 0$) and in the ferromagnetic insulator EuS ($z < -d$),

$$-\frac{D}{2}[\check{g},\partial_z\check{g}] = \begin{cases} 0, & z = 0, \\ -i[\tau_3\hat{v},\check{g}], & z = -d, \end{cases} \tag{A3}$$

where $\hat{v}(x,y) = -\frac{1}{2}Jn_{\rm 2D}\hat{\boldsymbol{\sigma}}\cdot\boldsymbol{S}(x,y)$. Thus the polarization of the superconductor is intimately connected with the magnetic structure of the EuS film through the quantity $\hat{v}(x,y)$ in Eq. (A3).

Despite the fact that the exchange field $\hat{h}_{\rm ex}(\boldsymbol{r})$ is strongly localized at the lower surface of the Al film, the tunneling density of states probed on the upper surface is modified by $\hat{h}_{\rm ex}(\boldsymbol{r})$ equally strongly as on the lower surface, provided d is small compared to the superconducting correlation length. Specifically, if $\hat{v} \ll D/d$, we find that the Green function on the upper surface ($\check{g}_0$) satisfies a 2D version of the Usadel equation, which differs from Eq. (1) only by a reduced dimensionality ($\alpha = x,y$) and an effective exchange field $\hat{h} \to \hat{h}_{\rm eff}(x,y)$ The magnetic structure of EuS can, therefore, be probed through a relatively thick Al layer ($d \lesssim \xi_0$), by studying, e.g., the superconducting density of states at excitation energies $E \lesssim \Delta$. Strictly speaking, in the vicinity of sharp domain walls, a steplike change of $\hat{v}(x,y)$ is imaged on the upper Al surface as a gradual transition over a length scale d.

[1] A. Mauger and C. Godart, Phys. Rep. **141**, 51 (1986).
[2] X. Hao, J. S. Moodera, and R. Meservey, Phys. Rev. B **42**, 8235 (1990).
[3] J. S. Moodera, T. S. Santos, and T. Nagahama, J. Phys.: Condens. Matter **19**, 165202 (2007).
[4] J. S. Moodera, G.-X. Miao, and T. S. Santos, Phys. Today **63**, 46 (2010).
[5] J. S. Moodera, X. Hao, G. A. Gibson, and R. Meservey, Phys. Rev. Lett. **61**, 637 (1988).
[6] P. M. Tedrow, J. E. Tkaczyk, and A. Kumar, Phys. Rev. Lett. **56**, 1746 (1986).
[7] P. Wei, S. Lee, F. Lemaitre, L. Pinel, D. Cutaia, W. Cha, F. Katmis, Y. Zhu, D. Heiman, J. Hone, J. S. Moodera, and C.-T. Chen, Nat. Mater. **15**, 711 (2016).
[8] P. Wei, F. Katmis, B. A. Assaf, H. Steinberg, P. Jarillo-Herrero, D. Heiman, and J. S. Moodera, Phys. Rev. Lett. **110**, 186807 (2013).
[9] J. Linder and J. W. A. Robinson, Nat. Phys. **11**, 307 (2015).
[10] F. S. Bergeret, A. F. Volkov, and K. B. Efetov, Rev. Mod. Phys. **77**, 1321 (2005).
[11] F. S. Bergeret, A. F. Volkov, and K. B. Efetov, Phys. Rev. Lett. **86**, 4096 (2001).
[12] A. Ozaeta, P. Virtanen, F. S. Bergeret, and T. T. Heikkilä, Phys. Rev. Lett. **112**, 057001 (2014).
[13] P. Machon, M. Eschrig, and W. Belzig, Phys. Rev. Lett. **110**, 047002 (2013).
[14] S. Kolenda, M. J. Wolf, and D. Beckmann, Phys. Rev. Lett. **116**, 097001 (2016).

[15] F. Giazotto, J. W. A. Robinson, J. S. Moodera, and F. S. Bergeret, Appl. Phys. Lett. **105**, 062602 (2014).
[16] F. Giazotto, T. T. Heikkilä, and F. S. Bergeret, Phys. Rev. Lett. **114**, 067001 (2015).
[17] D. Huertas-Hernando, Y. V. Nazarov, and W. Belzig, Phys. Rev. Lett. **88**, 047003 (2002).
[18] F. Giazotto and F. S. Bergeret, Appl. Phys. Lett. **102**, 162406 (2013).
[19] F. Giazotto and F. S. Bergeret, Appl. Phys. Lett. **102**, 132603 (2013).
[20] F. Giazotto, F. Taddei, R. Fazio, and F. Beltram, Appl. Phys. Lett. **89**, 022505 (2006).
[21] F. Giazotto, F. Taddei, R. Fazio, and F. Beltram, Phys. Rev. Lett. **95**, 066804 (2005).
[22] F. Giazotto and F. Taddei, Phys. Rev. B **77**, 132501 (2008).
[23] F. Giazotto, T. T. Heikkilä, A. Luukanen, A. M. Savin, and J. P. Pekola, Rev. Mod. Phys. **78**, 217 (2006).
[24] S. Kawabata, A. Ozaeta, A. S. Vasenko, F. W. J. Hekking, and F. S. Bergeret, Appl. Phys. Lett. **103**, 032602 (2013).
[25] F. Giazotto, P. Solinas, A. Braggio, and F. S. Bergeret, Phys. Rev. Appl. **4**, 044016 (2015).
[26] D. Aasen, M. Hell, R. V. Mishmash, A. Higginbotham, J. Danon, M. Leijnse, T. S. Jespersen, J. A. Folk, C. M. Marcus, K. Flensberg, and J. Alicea, Phys. Rev. X **6**, 031016 (2016).
[27] C. Beenakker and L. Kouwenhoven, Nat. Phys. **12**, 618 (2016).
[28] Y. M. Xiong, S. Stadler, P. W. Adams, and G. Catelani, Phys. Rev. Lett. **106**, 247001 (2011).
[29] B. Li, G.-X. Miao, and J. S. Moodera, Phys. Rev. B **88**, 161105 (2013).
[30] P. Tischer, IEEE Trans. Magn. **9**, 9 (1973).
[31] K. D. Usadel, Phys. Rev. Lett. **25**, 507 (1970).
[32] N. Moussy, H. Courtois, and B. Pannetier, EPL **55**, 861 (2001).
[33] H. le Sueur, P. Joyez, H. Pothier, C. Urbina, and D. Esteve, Phys. Rev. Lett. **100**, 197002 (2008).
[34] R. Meservey and P. M. Tedrow, Phys. Rep. **238**, 173 (1994).